Modelling the time-dependent mechanical properties of thermoplastic and thermosetting polymers with Gumbel distribution functions

Virág Á. D., Molnár K.

Polymer 312 (2024) 127642

Contents lists available at ScienceDirect

Polymer

journal homepage: www.elsevier.com/locate/polymer

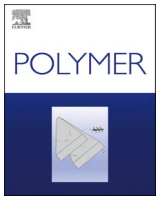

Modelling the time-dependent mechanical properties of thermoplastic and thermosetting polymers with Gumbel distribution functions

Ábris Dávid Virág [a], Kolos Molnár [a,b,*]

[a] Department of Polymer Engineering, Faculty of Mechanical Engineering, Budapest University of Technology and Economics, Műegyetem Rkp. 3., H-1111, Budapest, Hungary
[b] ELKH–BME Research Group for Composite Science and Technology, Műegyetem Rkp. 3., H-1111, Budapest, Hungary

ARTICLE INFO

Keywords:
Creep
Stress relaxation
Master curve
TTS
Plasticiser

ABSTRACT

In this paper, we propose a simple modelling method that accurately describes the time-dependent viscoelastic behaviour of thermoplastic and thermosetting solid polymers. We performed short-term creep and stress relaxation tests on representative samples of three major classes of polymers: an amorphous, a semi-crystalline thermoplastic and a thermosetting polymer. Then, to investigate the relationship between the model parameters and the material composition, we also tested thermoplastic matrix composites with different plasticiser contents. From the short-term tests, master curves were constructed with the use of the time–temperature superposition principle. Then, the temperature dependence of the obtained shift factors was described using the Arrhenius model. The resulting creep compliance and relaxation modulus master curves were normalised and modelled with a two-parameter cumulative Gumbel distribution function (CDF) and its complementary distribution function (CCDF). For the creep and stress relaxation master curves, the median error of modelling was less than 16 % and 16.5 % in all cases, respectively. Furthermore, it was less than 2 % for the thermosetting polymer, making this model an excellent tool for describing the creep and stress relaxation behaviour of thermosetting systems. In the case of the plasticised composites, we found a strong relationship between the material composition and the location parameter of the Gumbel model. Based on this, we developed a method that can be used to estimate the evolution of the creep compliance curve for any arbitrary OLA content (between 0 wt% and 16 wt%) at any desired temperature (between 22 °C and 70 °C).

1. Introduction

Various viscoelastic materials, such as polymers, bitumens, or biological tissues, are used in engineering practice. These materials exhibit both solid-like and liquid-like properties in the solid state, and their stress–strain relationship is time- and temperature-dependent. Time dependency can be observed in time-dependent deformation under constant load (called creep or strain relaxation) and in time-dependent decrease in stress under constant strain (called stress relaxation).

Design methods for engineering structures made of viscoelastic materials usually take viscoelastic properties into account. This is particularly important in cases where the product is designed to last for decades, such as sewer pipes [1], power plant components [2] or reactor elements [3]. However, 30- or 40-year-long tests are not feasible.

Fortunately, temperature and time similarly affect the mechanical properties of viscoelastic materials. Therefore, increasing the temperature can accelerate creep or stress relaxation. The time required to characterise the long-term mechanical behaviour of viscoelastic materials can be significantly reduced. The utilisation of these analogous effects to reduce the characterisation time is called the time–temperature superposition (TTS) principle [4,5].

To apply these time-dependent characteristics to design, we need closed-form mathematical models that can describe the time dependence of creep or stress relaxation with sufficient accuracy, even for decades of prediction. One of the most commonly used methods is to model the polymer as a network of springs and dashpots connected in series and/or parallel with classic viscoelastic models, such as the Maxwell, Kelvin-Voigt or Standard-Solid models [6,7]. However, the disadvantage of these models is that for accurate description, usually generalised models are needed, in which multiple such models are

* Corresponding author. Department of Polymer Engineering, Faculty of Mechanical Engineering, Budapest University of Technology and Economics, Műegyetem Rkp. 3., H-1111, Budapest, Hungary.
E-mail addresses: viraga@pt.bme.hu (Á.D. Virág), molnar@pt.bme.hu (K. Molnár).

https://doi.org/10.1016/j.polymer.2024.127642
Received 21 June 2024; Received in revised form 7 September 2024; Accepted 18 September 2024
Available online 22 September 2024

connected in parallel and/or in series. In this case, the number of fitted parameters can be sometimes up to 40 or even more [8]. Therefore, the fitting becomes a rather complicated process that requires optimisation algorithms.

There are different approaches to this optimisation. Barrientos et al. [9] proposed an optimisation method for fitting the generalised Maxwell model, represented by a Prony series that distributes the time coefficients along the time scale to achieve the best fit. Cui et al. [10] proposed a two-step optimisation for Prony-series fitting by combining the linear least square solver and the particle swarm optimisation method. These methods require significant computational capacity.

The use of fractional models can be a solution to reduce the number of fitting parameters. Fractional models also describe the material's behaviour with a network of mechanical elements, but in addition to the spring and the dashpot, we use an additional (fractional) element, the so-called springpot [11]. Another option is to use empirical models, the most common being Findley's and Norton's power law. These methods have the advantage of containing only a few parameters but only work well if the investigated material exhibits power-law behaviour [12]. Several other modelling methods can be used to describe viscoelastic behaviour as a function of time, such as the Kohlrausch–Williams–Watt (KWW) stretched exponential function [12], viscoelastic models containing an active element with changing resting length (Muñoz element) [13,14] or even artificial neural network–based methods [15]. However, most existing modelling methods either have complex fitting algorithms and, therefore, require extensive computational resources, or only give an accurate description over a limited range.

This paper proposes a modelling method that can describe the time-dependent viscoelastic behaviour of thermoplastic and thermosetting solid polymers over a long time (up to decades) with low computational capacity. Short-term creep and stress relaxation tests were performed on an amorphous and a semi-crystalline thermoplastic, a thermoset, and plasticised, short fibre–reinforced amorphous thermoplastic polymer. From the short-term tests, master curves were created using the TTS principle. The resulting creep compliance and relaxation modulus master curves were normalised and modelled with a cumulative Gumbel distribution function (CDF) and its complementary function (CCDF), respectively. We present that the Gumbel model is suitable to describe the long-term behaviour of various polymeric materials. Also, we found that the parameters of the Gumbel model can be associated with the material composition.

2. Materials and methods

2.1. Materials and sample preparation

Regarding their molecular structure, polymers can be linear or cross-linked, amorphous or semi-crystalline [16]. In terms of viscoelastic behaviour, three classes can be defined that exhibit distinctly different time-dependent behaviour [4]: amorphous thermoplastic, semi-crystalline thermoplastic and thermosetting polymers. To test the general applicability of the method proposed, we have chosen a representative, widely used material from each class. Also, multi-phase composite materials are commonly used in engineering practice [17]. Therefore, we also investigated short-fibre-reinforced composite materials with amorphous thermoplastic matrix.

For the amorphous thermoplastic class, we chose a commodity polymer, polystyrene (PS). The PS used was a general-purpose grade, Edistir N 3840 (supplied by Versalis, San Donato Milanese, Italy) and chose injection moulding for processing. The semi-crystalline thermoplastic polymer we chose was one of the most promising biopolymers [18] that is currently produced in the largest amount [19], polylactic acid (PLA). We used an extrusion-grade material, Ingeo 4032D (supplied by NatureWorks LLC, Plymouth, MN, USA), with a D-lactide content of 1.4–2% [20]. An epoxy acrylate–based material (EPA), VeroWhitePlus (RGD835) (supplied by Stratasys, Eden Prairie, MN, USA), was chosen as

Table 1
Details of sample preparation.

Material	Details of sample preparation
Amorphous thermoplastic: PS (Edistir N 3840)	• Processing technology: injection moulding, • machine: Arburg Allrounder Advance 270S 400–170 (Arburg GmbH, Lossburg, Germany), • mould: conventional two-cavity cold-runner mould for type 1A dumbbell-shape specimens (ISO 527–2:2012), • processing parameters (according to the manufacturer's recommendations): feed zone temperature: 40 °C, barrel temperatures: 205–220 °C, mould temperature: 30 °C, shot volume: 45 cm^3, injection rate: 44 cm^3/s.
Semi-crystalline thermoplastic: PLA (Ingeo 4032D)	• Processing technology: injection moulding, • before processing: drying (according to the manufacturer's recommendations) at T = 80 °C for 4 h, • machine: Arburg Allrounder Advance 270S 400–170 (Arburg GmbH, Lossburg, Germany), • mould: conventional two-cavity cold-runner mould for type 1A dumbbell-shape specimens (ISO 527–2:2012), • processing parameters (according to the manufacturer's recommendations): feed zone temperature: 40 °C, barrel temperatures: 185–200 °C, mould temperature: 30 °C, shot volume: 45 cm^3, injection rate: 44 cm^3/s, • post-crystallisation heat-treatment (based on the work of Yoo et al. [22]) at T = 100 °C for 1 h (between metal sheets to avoid warping).
Thermoset: EPA (VeroWhitePlus)	• Processing technology: 3D printing (PolyJet technology), • machine: Objet 30 Pro (Stratasys, Eden Prairie, MN, USA), • specimen geometry: 60 mm length with a cross-section of 2 × 10 mm^2, • processing parameters: automatically generated by the printer's software, according to the material chosen; matte surface finish.
Short-fibre-reinforced amorphous plasticised thermoplastic composite: PLA+CF30+OLA (Ingeo 4060D+ Panex 35 chopped fibre (Type-95))	• Processing technology: extrusion + compression moulding, • before processing: drying (according to the manufacturer's recommendations) the PLA at T = 45 °C for 6 h, • extrusion (based on our previous study [23]): • 1st compounding: PLA+OLA using LTE 24–44 twin-screw extruder and an LDF-1.6 liquid dosing system (Labtech Engineering, Samutprakarn, Thailand) at 0, 4, 8 and 16 wt% OLA contents; zone temperatures: 180–190 °C (0 and 4 wt %), 150–160 °C (8 wt%), 140–150 °C (16 wt%); screw L/D ratio: 44 mm, screw diameter: 26 mm, screw speed: 40 rpm • monofilament cooling on conveyor belt into an LZ-120/VS granulator (2.5-mm-long pellets), • 2nd compounding: plasticised pellets (PLA+OLA) with the fibres at 30 wt% (CF30) using LTE 24–44 twin-screw extruder, zone temperatures: zone temperatures: 180–190 °C (0 and 4 wt% OLA), 150–160 °C (8 wt% OLA), 140–150 °C (16 wt% OLA); screw speed: 25 rpm,

(*continued on next page*)

Table 1 (*continued*)

Material	Details of sample preparation
	• monofilament cooling on conveyor belt into an LZ-120/VS granulator (6-mm-long pellets), • compression moulding • hot press machine: Line Platen Press 200E (Dr. Collin GmbH, Munich, Germany), • parameters: die: 160 mm × 160 mm sheets with 2 mm thickness, temperature: 180 °C, pressure: 20 MPa maximum hydraulic pressure (pressure on the sample surface was 2.5 MPa).

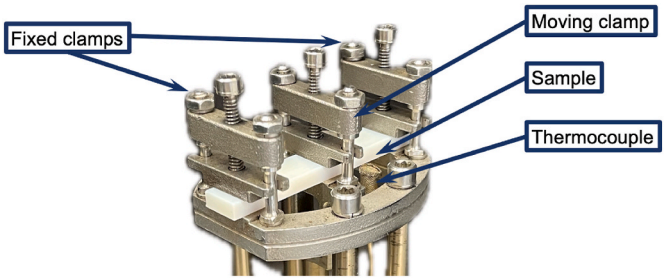

Fig. 1. DMA test setup with dual cantilever clamp.

the thermosetting material and these specimens were generated by 3D printing. In the case of the composite material, the matrix material was an amorphous thermoplastic PLA, Ingeo 4060D (supplied by NatureWorks LLC, Plymouth, MN, USA), with a D-lactide content of 12–12.3 % [20]. The reinforcing material was chopped carbon fibre, Panex 35 (Type-95) (supplied by Zoltek Zrt, Nyergesújfalu, Hungary), with a diameter and length of 8.3 μm and 6 mm, respectively. We chose compression moulding for specimen preparation from this type of material.

Carbon fibre-reinforced PLA composites are widely used for 3D printing as PLA is easy to print and, with the addition of carbon fibres, functional properties (such as electrical conductivity) can be achieved [21]. However, as fibres increase viscosity, the addition of plasticisers is necessary to ensure printability. To investigate the relationship between the model parameters and the material composition, a plasticiser was added to the short fibre composite at different weight ratios. Glyplast OLA2 (Condensia, Barcelona, Spain) oligomeric lactic acid (OLA) was chosen to prepare plasticised composites with 0, 4, 8 and 16 wt% (wt%) plasticiser contents. The applied processing technologies and the main details of sample preparation are listed in Table 1.

2.2. Creep and stress relaxation tests

Creep and stress relaxation tests were performed with a TA Q800 (TA Instruments, New Castle, DE, USA) dynamic mechanical analyser (DMA) using a dual cantilever clamp (Fig. 1). The specimens were 60 mm long in all cases. The amorphous and semi-crystalline thermoplastic polymers (PS, PLA) produced by injection moulding had a cross-section of 4 mm × 10 mm. In the other cases (EPA, PLA composites), tests were performed on specimens with a cross-section of 2 mm × 10 mm. The ASTM 5418 standard does not specify the preferred sample size. Therefore, sample sizes were chosen according to the recommendations of the DMA Q800 instrument's user manual. The user manual states that in the case of unreinforced thermoplastics, thermosets and composites, the length/thickness ratio of the test specimens should be at least 10 for the dual cantilever clamp. It was also important to ensure that the modulus and compliance values fell within the operating range of the dual cantilever clamp.

Table 2
The creep and stress relaxation tests performed.

Material	T_g (°C)	15-min-long test temperatures (°C)		180-min-long validation test temperatures (°C)	
		Creep	Stress relaxation	Creep	Stress relaxation
PS (amorphous thermoplastic)	91.6	30, 40, 50, 60, 70, 80, 83, 86, 90, 95, 100	27, 40, 50, 55, 60, 70, 75, 80	60, 80	70, 80
PLA (semi-crystalline thermoplastic)	64.6	26, 30, 40, 50, 60, 65, 70, 80, 95, 110, 130, 150	24, 40, 50, 55, 60, 65, 70, 80, 95, 110, 130, 150	50, 70	–
EPA (thermoset)	55.9	27, 32, 40, 50, 60, 70	28, 33, 36, 40, 50, 70	33	–
PLA+CF30+OLA0 (thermoplastic composite)	57.9	26, 40, 45, 50, 53, 55, 60	–	–	–
PLA+CF30+OLA4 (plasticised thermoplastic composite)	56.5	40, 50, 55, 60, 70	–	–	–
PLA+CF30+OLA8 (plasticised thermoplastic composite)	48.8	25, 40, 50, 55, 60	–	–	–
PLA+CF30+OLA16 (plasticised thermoplastic composite)	38.6	22, 26, 35, 40	–	–	–

In a creep or stress relaxation test, the material is subjected to constant stress or strain excitation, respectively. Tests were performed with excitation load levels within the linear viscoelastic region (LVER). From an experimental point of view, the load level is within the LVER if the relaxation modulus or creep compliance curves obtained at two different load levels coincide. In the LVER, the applied excitation load is sufficiently small. Therefore, the deviation of molecules from their equilibrium state is negligible. In this region, the creep compliance or relaxation modulus is independent of the excitation load level.

To confirm that tests were performed within the LVER at each temperature, we performed 5-min-long tests at different loads. Then, we compared the resulting creep compliance or stress relaxation curves. If the maximum deviation between the resulting two time-dependent creep or stress relaxation curves obtained at different loads was less than 5 %, both loads were considered to be within the LVER. Then, the higher load was used.

Our aim was to characterise the complete creep and stress relaxation behaviour in the solid state. These can be achieved by constructing a master curve based on the time-temperature superposition (TTS) principle [5].

For this purpose, we carried out 15-min-long tests (during which 896 data points were recorded). To validate our master curves to a certain extent, we performed 180-min-long tests. Before the tests, a 5-min soak time was used at the test temperature to achieve thermal equilibrium and allow relaxation. The parameters of the tests performed are shown in Table 2.

For proper solid-state characterisation, the glass transition temperature (T_g) had to be taken into account. Polymers are in their glassy state below their T_g. As segmental movements are induced around T_g, the material's resistance to deformation is reduced. Therefore, amorphous

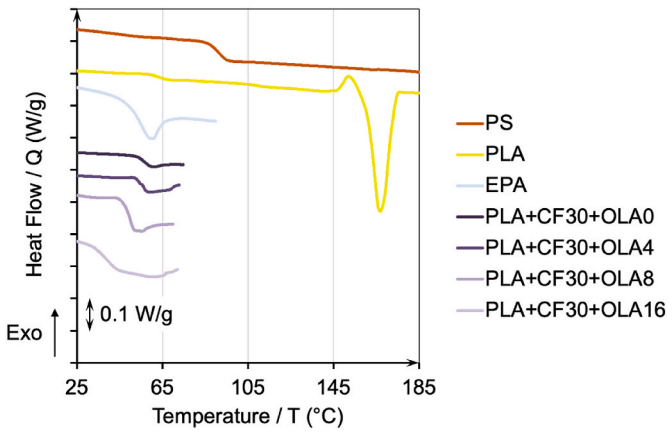

Fig. 2. DSC curves of the amorphous thermoplastic PS, the semi-crystalline thermoplastic PLA, the thermosetting EPA and the plasticised composite materials.

polymers above T_g are in their rubbery state [24]. To describe the behaviour of the material in its solid state, we have to know its behaviour in both its glassy and its rubbery state. Therefore, we performed creep and stress relaxation tests above and below T_g. During the selection of the materials, we ensured that their T_g values were well above room temperature. Therefore, tests under room temperature were not necessary.

To determine the T_g of the tested materials, we performed differential scanning calorimetry (DSC) using a Q2000 (TA Instruments, New Castle, DE, USA) device. The weight of the samples was 8–10 mg. We applied a single heat cycle of 0–200 °C, 0–200 °C, 0–90 °C and 0–70 °C with a heating rate of 10 °C/min for the PS, PLA, EPA and PLA + CF30 + OLA composites, respectively. Using the TA Universal Analysis software, we determined T_g as the midpoint of the step in the heat flow curves (Fig. 2). The calculated T_g values are shown in Table 2.

Fig. 2 shows that in case of the composite materials, increasing plasticiser content led to a decrease in T_g. This is expected, as the small molecule plasticiser prevents the formation of secondary bonds between the chains of the polymer, thus increasing the mobility of the chains. The onset temperature of the melting peak for semi-crystalline PLA is around 150 °C. Therefore, this was chosen as the maximum test temperature for

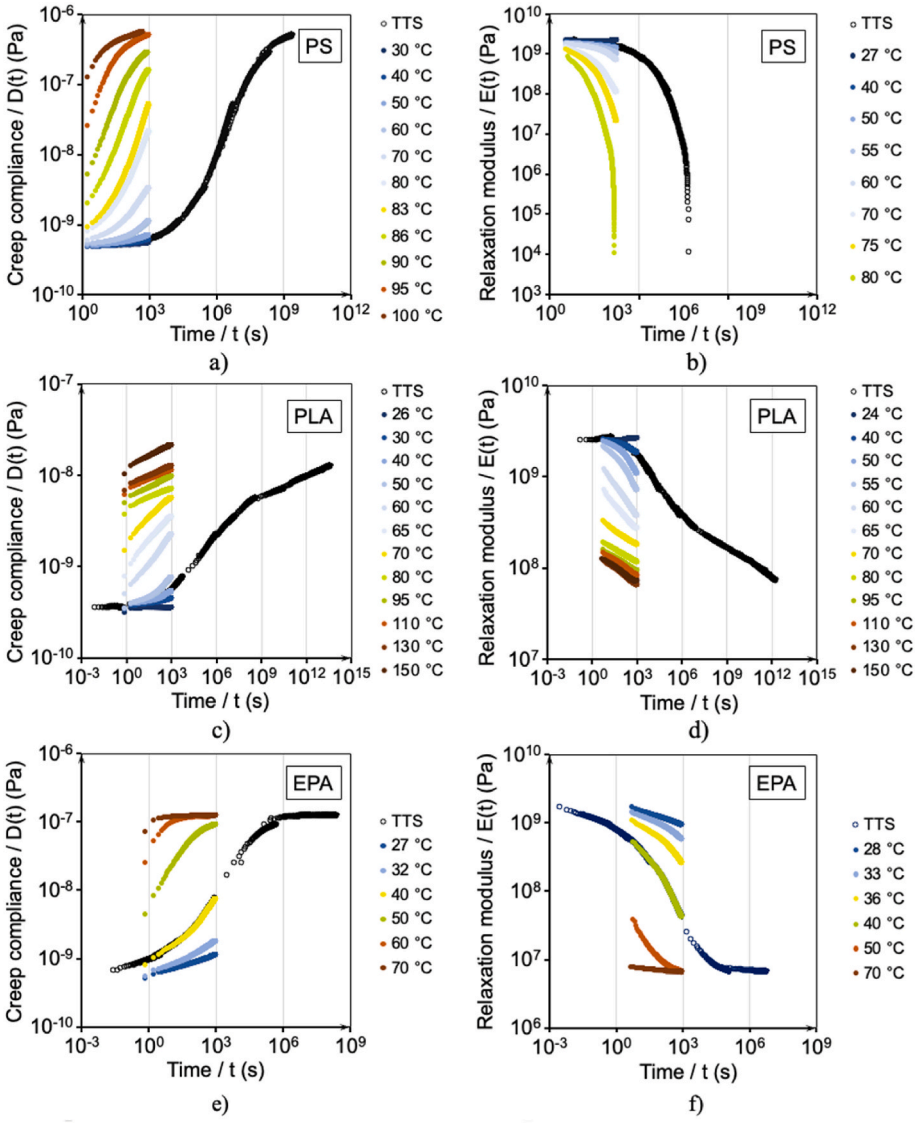

Fig. 3. Master curves generated from creep and stress relaxation measurements for the amorphous thermoplastic PS (a,b), the semi-crystalline thermoplastic PLA (c, d) and the thermosetting EPA (e,f) based on the TTS principle at T_{ref} = 40 °C in double logarithmic scale.

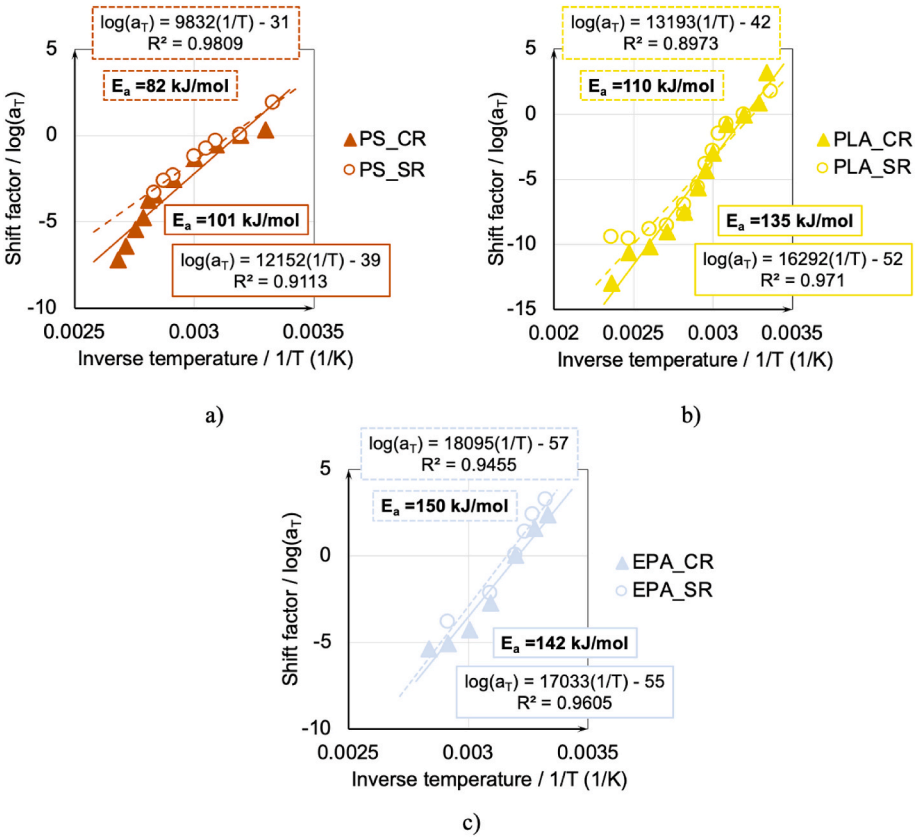

Fig. 4. Arrhenius plots of the shift factors used to generate the creep compliance and relaxation modulus master curves for the amorphous thermoplastic PS (a), the semi-crystalline thermoplastic PLA (b) and the thermosetting EPA (c) in double linear scale. Full markers and continuous lines stand for creep (CR), and empty markers and dashed lines stand for stress relaxation (SR).

PLA. The degree of crystallinity (X_C) of the semi-crystalline PLA was determined by Eq. (1):

$$X_C(\%) = \frac{\Delta H_m - \Delta H_{cc}}{\Delta H_m^0} \cdot 100, \quad (1)$$

where ΔH_m is the crystal melting enthalpy calculated as the area under the melting peak, ΔH_{cc} is the cold crystallisation enthalpy calculated as the area under the cold crystallisation peak and $\Delta H_m^0 = 93$ J/g [25] is the crystal melting enthalpy of 100 % crystalline PLA. Based on Eq. (1), X_C = 39 % for the semi-crystalline PLA.

2.3. Master curve generation and model fitting

From the 15-min-long tests, we obtained the time-dependent creep compliance and stress relaxation curves, and used them to generate master curves in the IRIS Rheo-hub 2023 software based on the temperature–time superposition (TTS) principle [5,26]. To obtain a continuous curve at the chosen reference temperature the software minimises the discrepancy between overlapping sections of the shifted curves. For the generation of the master curves, only horizontal shift factors (a_T) were used, and the curves were shifted to the reference temperature T_{ref} = 40 °C. The data for a viscoelastic characteristic measured at T_1 temperature and t_1 time, (e.g. the relaxation modulus ($E(T_1, t_1)$) can be converted to data at the reference temperature using linear variable transformation. For the conversion, a horizontal shift factor (a_T) is used, which considers the effect of temperature on modulus (Eq. (2)):

$$E(T_1, t_1) = E\left(T_{ref}, \frac{t_1}{a_T}\right). \quad (2)$$

The resulting master curves were used for the model fits described in Section 3.3. The temperature dependence of the shift factors can be described using the Arrhenius-equation (Eq. (3)):

$$\log a_T = \frac{E_a}{R} \cdot \left(\frac{1}{T} - \frac{1}{T_{ref}}\right) \quad (3)$$

where E_a (J/mol) is the activation energy, and R is the universal gas constant (R = 8.314 J/molK). To obtain the activation energy, we fitted a linear trend ($\log a_T = A\ (1/T) + B$) to the $\log a_T\ (1/T)$ dependence and calculated the activation energy from the slope of the trend as: $E_a = (A \cdot R)$. All model fittings were carried out in Wolfram Mathematica 13.1. For the modelling of the TTS curves we applied the "NonlinearModelFit", "CDF" "GumbelDistribution" and "SurvivalFunction" built-in algorithms.

3. Results and discussion

3.1. Generation and validation of master curves for different types of polymers

Fig. 3 shows the 15-min-long creep and stress relaxation curves and the master curves generated from these data. In all the cases, the reference temperature was chosen to be 40 °C 40 °C is a typical ambient temperature in the environment of a component that emits thermal energy in an operating devic e, such as a motor or a lamp tube [27–29]. We can see that the master curves are continuous, meaning superposition was successful [30].

The master curves generated from the 10^3 s tests can be used to predict the creep and relaxation behaviour of the tested materials up to 10^9 s (≈32 years) at T = 40 °C, except for the stress relaxation behaviour

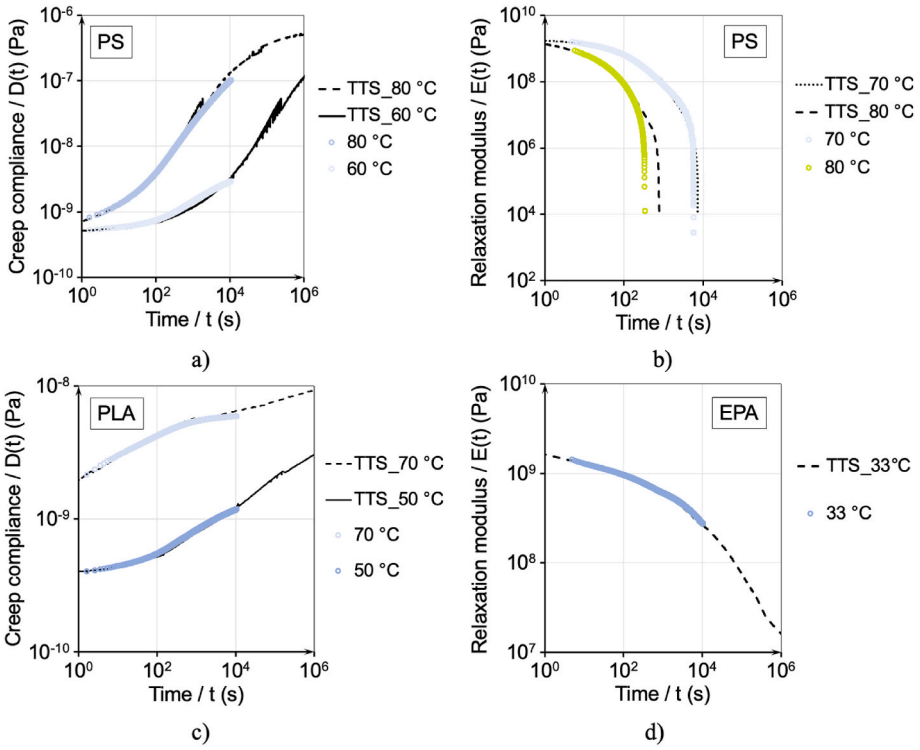

Fig. 5. Validation of master curves for the amorphous thermoplastic PS (a,b), the semi-crystalline thermoplastic PLA (c) and the thermosetting EPA (d) materials constructed from 15-min tests using 3-h-long tests in double logarithmic scale.

of the amorphous thermoplastic PS. In this case, the relaxation modulus decreased by 5 orders of magnitude even at very low strain excitation during the 15-min test at $T = 80$ °C, and the material showed a gel-like/liquid-like behaviour. Therefore, the PS could not be tested at higher temperatures for stress relaxation. This narrower range of investigation (compared to the creep tests) is related to the inevitable sudden initial deformation of the stress relaxation test. The material is much more sensitive to a small change in the strain excitation applied for stress

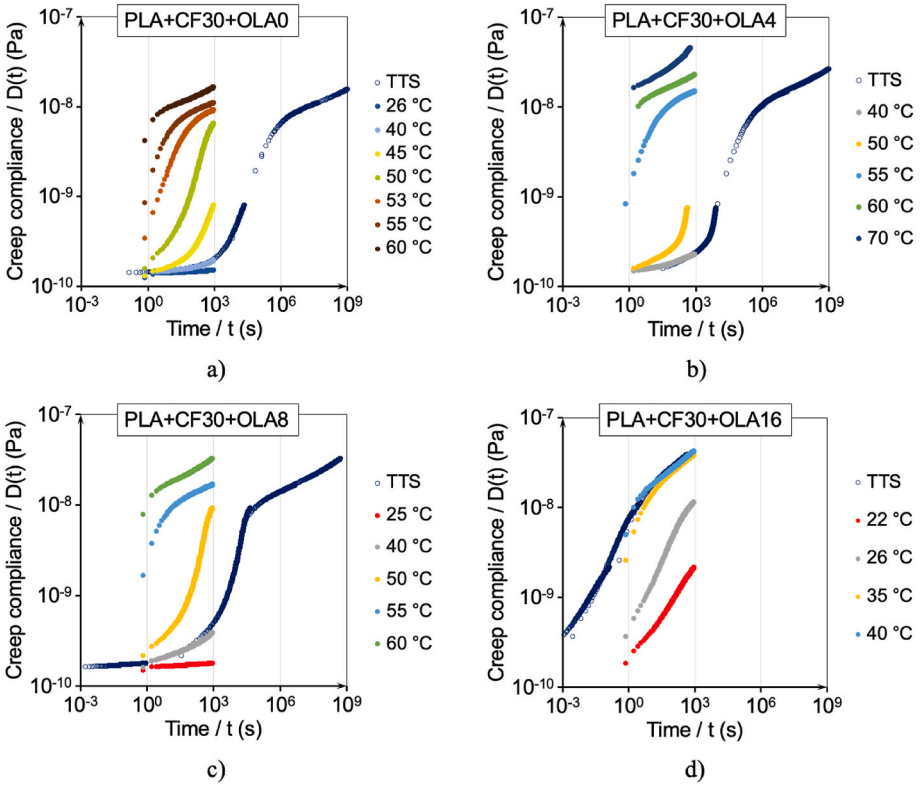

Fig. 6. Master curves generated from creep measurements for the plasticised composites based on the TTS principle at $T_{ref} = 40$ °C in double logarithmic scale.

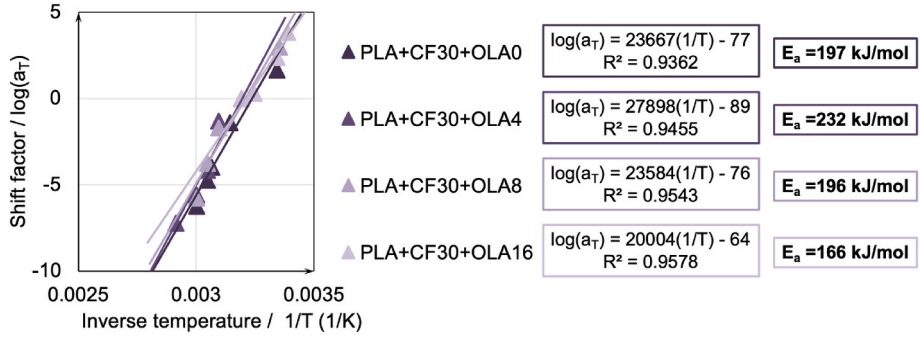

Fig. 7. Arrhenius plots of the shift factors used to generate the creep compliance master curves for the plasticised composites in double linear scale.

relaxation measurements than a small change in the stress excitation applied for creep measurements. In the case of thermosetting EPA, the creep and stress relaxation master curves do not reach 10^9 s. Still, from 10^6 s (≈12 days), these curves are quasi-constant, and due to the cross-linked structure of the material, it can be assumed that this constancy will remain until decomposition [4].

The generated master curves predict the evolution of creep compliance and relaxation modulus over time for nearly 32 years. Of course, in real application conditions, these results must be treated with care. Besides thermal exposure, other factors such as chemical exposure, humidity, UV radiation, etc., also affect the components, all of which influence the behaviour of the polymer in different ways.

The temperature dependence of the shift factors was plotted on Arrhenius plots (Fig. 4). In all cases, the Arrhenius model can properly describe the temperature dependence of the shift factors. We also calculated the activation energies (E_a) from the slope of the fitted curves. As expected, the E_a values from the creep and relaxation master curves of the same material resulted in similar values. The values obtained for each material (Fig. 4) are in good agreement with the literature data (PS [31], PLA [32], EPA [33]).

The master curves are used to make predictions over a long period of time, so their validation is quite challenging. It is impractical to carry out measurements over several months or even years, as it is very energy- and resource-intensive and would significantly increase the duration and cost of a product's design phase.

Therefore, we performed 180-min-long validation tests, which were 12 times longer than the original tests. In this way, we provide partial validation for up to one decade (on the logarithmic time scale), from 10^3 to 10^4 s. The validation tests were carried out at temperatures at which an order of magnitude change in creep compliance or relaxation modulus had already occurred during the original tests (see Table 2).

Validation tests were performed for all three materials (Fig. 5). Using the shift factors plotted in Fig. 4, the generated master curves were shifted to the temperatures of the validation tests. Fig. 5 shows that at the 10^3–10^4 s region, the creep and relaxation behaviour of the examined materials agrees with those predicted by the master curves. The only major difference is at the relaxation modulus of PS at $T = 80$ °C, where a large drop in modulus occurs 7 min earlier than expected from the master curve. The results suggest that these master curves provide reliable predictions.

3.2. Generation of master curves for plasticised composites with different composition

We performed the master curve generation to $T_{ref} = 40$ °C for the composite materials (Fig. 6). The creep behaviour at $T_{ref} = 40$ °C can be predicted up to several decades for the composites containing 0, 4 and 8 wt% plasticiser (even up to 32 years for 0 and 4 wt% cases). In these three cases, the glass transition region (the steepest part of the curves) falls between 10^3 and 10^6 s, whereas in the 16 wt% case, it starts much earlier and falls roughly between 10^3 and 10° s. This is consistent with the DSC results since the T_g of the PLA + CF30 + OLA16 is 38.6 °C, i.e. in this case, $T_{ref} = 40$ °C is already higher than the T_g of the material (Table 2).

We presented the temperature dependence of the shift factors on an Arrhenius plot (Fig. 7) for the composites as well. The figure shows that the Arrhenius model can properly describe the temperature dependence of the obtained shift factors. Moreover, all the shift factors fall approximately in a single trend. Consequently, the plasticiser content did not affect the temperature dependence of the shift factors. Overall, it can be stated that the E_a for these composite systems is around 200 kJ/mol.

3.3. Modelling method based on gumbel distribution

The total creep compliance and relaxation modulus curves of solid polymers are similar to a cumulative distribution function (CDF) and its complementary function (CCDF). In this study, we propose a master curve modelling method using the Gumbel distribution function based on the work of Álvarez-Vázquez et al. [34]. The steps of the modelling method are shown in Fig. 8. For the modelling of the relaxation modulus master curve (Fig. 8/a), the first step is to normalise the time (t) and modulus (E) values (Fig. 8/b) to get the normalised time (t^*) and normalised relaxation modulus (E^*) and creep compliance (D^*) values. We

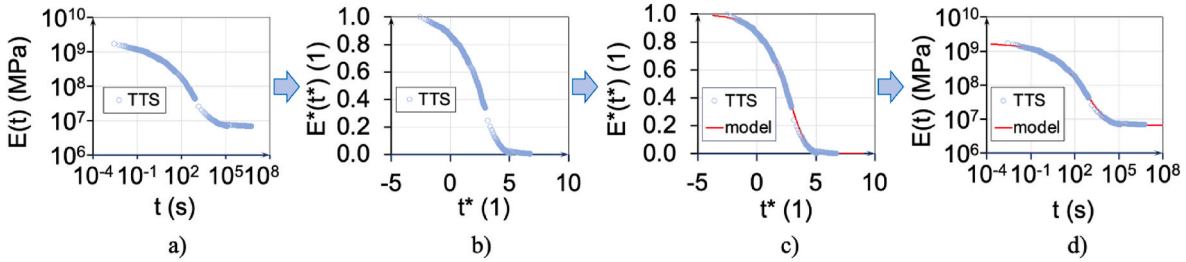

Fig. 8. Steps of the modelling method: master curve generation (represented in dobule logarithmic scale) (a), normalisation using Eqs. (4) and (5) (represented in double linear scale) (b), Gumbel CCDF (Eq. (7)) fitting (represented in double linear scale) (c), inverse normalisation to obtain time-dependent data (represented in double logarithmic scale) (d).

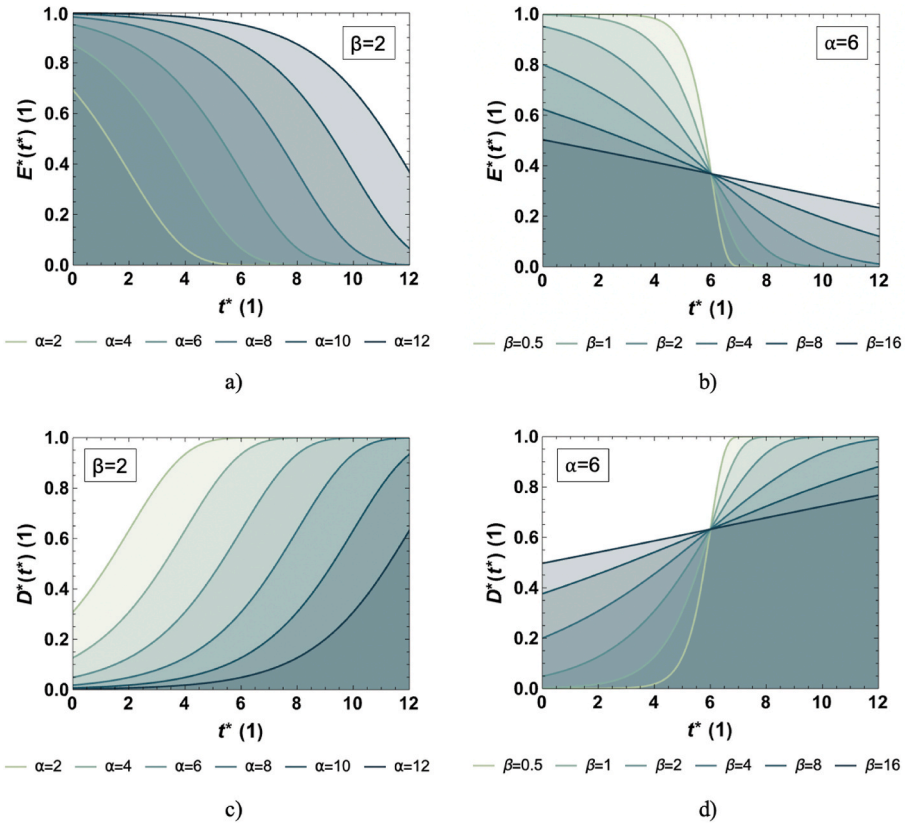

Fig. 9. Parametric study of the effect of the location (α) and scale (β) parameters of the Gumbel CCDF (Eq. (7)) (a,b) and the Gumbel CDF (Eq. (8)) models (c,d) using normalised values in double linear scale.

used the normalisation proposed by Álvarez-Vázquez et al. [34] (Eqs. (4)–(6)):

$$t^* = \log\left(\frac{t}{t_0}\right), \tag{4}$$

$$E^* = \frac{\log\left(\frac{E}{E_{min}}\right)}{\log\left(\frac{E_{max}}{E_{min}}\right)}, \tag{5}$$

$$D^* = \frac{\log\left(\frac{D}{D_{min}}\right)}{\log\left(\frac{D_{max}}{D_{min}}\right)}, \tag{6}$$

where $t_0 = 1$ s and E_{max}/D_{max} and E_{min}/D_{min} are the maximum and minimum modulus values of the $E(t)/D(t)$ master curve to be modelled, respectively. For each material, we have defined an upper limit below which the curves seem to follow the shape of the Gumbel distribution function. Above the threshold, the slope of the curve is usually too large, which cannot be accurately represented by the Gumbel function. Thus, the D_{max} for the creep compliance curves and the E_{max} the for the relaxation modulus curves are the upper and lower values of the curve segment used for modelling.

For the $E^*(t^*)$ and $D^*(t^*)$ curve, the Gumbel CCDF (Eq. (7)) and the Gumbel CDF (Eq. (8)) was fitted, respectively (Fig. 8c):

$$E^*(t^*) = 1 - e^{-e^{-\frac{t^*-\alpha}{\beta}}}, \tag{7}$$

$$D^*(t^*) = e^{-e^{-\frac{t^*-\alpha}{\beta}}}, \tag{8}$$

where α is the location, β is the scale parameter, and both are fitted. The goodness of fit was rated by the normalised root mean square error (NRMSE) (Eq. (9)):

$$NRMSE = \frac{\sqrt{\sum_{i=1}^{n} \frac{\left(X^*_{TTS,i} - X^*_{model,i}\right)^2}{n}}}{X^*_{TTS\_max,i}} \cdot 100\ (\%), \tag{9}$$

where n is the number of points of the master curve, X^*_{TTS} is the normalised modulus or compliance values of the master curve and X^*_{model} is the normalised modulus or compliance values calculated from the fitted model and $X^*_{TTS\_max}$ is the largest normalised modulus or compliance value of the master curve ($X^*_{TTS,max} = 1$).

Finally, values of the $E^*(t^*)$ or $D^*(t^*)$ model curve obtained as a result of fitting were transformed to $E(t)$ or $D(t)$ based on Eqs. (4)–(6). The advantage of this method is that it is easy to use, as in this case only two parameters need to be fitted, thus complex optimisation algorithms are not required.

3.4. The basis for using the gumbel distribution function

Gumbel CDF (Eq. (8)) and Gumbel CCDF (Eq. (7)) models fitted to creep compliance and relaxation modulus master curves have the advantage of having only two parameters (location and scale parameter). Thus, instead of large data sets describing the points of the master curve, only two parameters are required, making the resulting master curves easier to manage and analyse. The modelling can also help smooth out noise arising from measurement errors and overlapping parts of the master curve. Another advantage is that a close relationship between model parameters and material properties can be defined for samples having similar material composition. We performed a

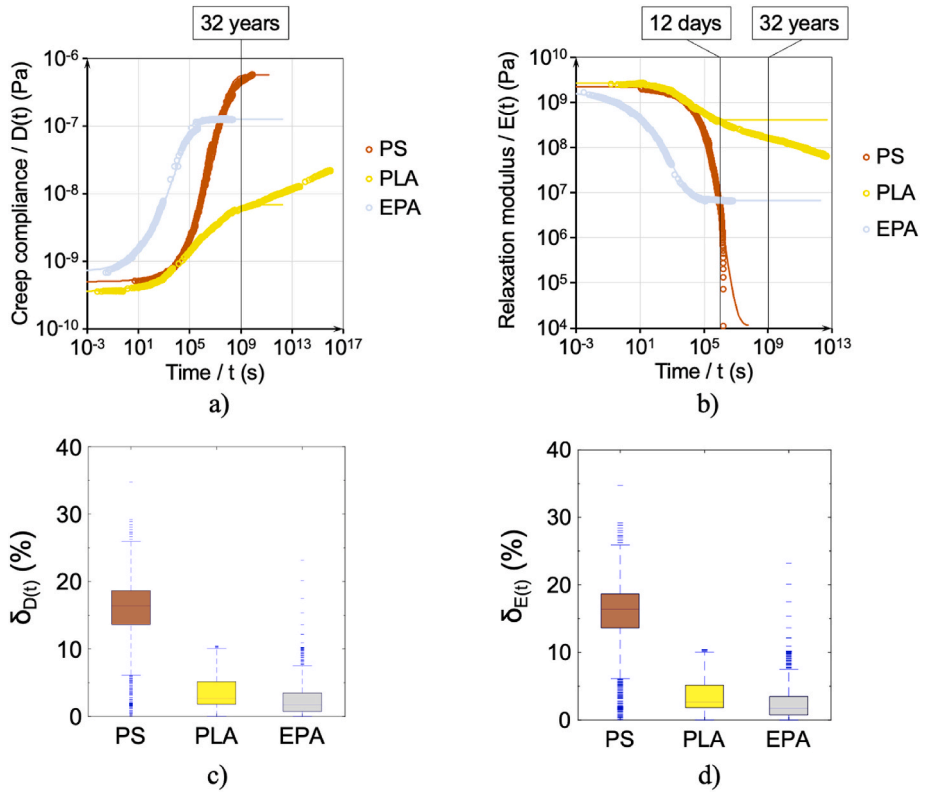

Fig. 10. Generated creep compliance (a) and relaxation modulus (b) master curves and models for the amorphous thermoplastic PS, the semi-crystalline thermoplastic PLA, the thermosetting EPA materials in double logarithmic scale, and box plots of percent error for creep (c) and stress relaxation (d) models. The empty circles denote the data points of the TTS curves, and the continuous lines represent the fitted models.

Table 3
Results of model fitting for the PS, PLA and EPA materials.

		Model fitting in the normalised field			Difference between TTS and model curve in real time
		Fitted parameters		NRMSE (%)	δ_{median} (%)
		α	β		
Creep	PS	6.859	1.301	2.5	12.5
	PLA	6.213	1.951	2.7	8.0
	EPA	3.768	1.553	1.1	1.5
Stress relaxation	PS	6.238	0.802	2.4	16.4
	PLA	4.326	0.999	2.4	2.7
	EPA	2.837	1.436	0.7	1.7

parametric study (Fig. 9) to illustrate the effect of the location and scale parameters and their relationship to material properties. For clarity, the data are presented for the time-dependent relaxation modulus and creep compliance in a normalised system.

Fig. 9a,c shows that, for a fixed scale parameter ($\beta = 2$), the model curves shift along the time axis as the location parameter (α) changes. α determines the location of the curve's inflexion point, which is usually associated with the glass transition. Consequently, this parameter can be used to track changes in any material property that does not affect the shape of the creep/relaxation curve but only has the effect of shifting the glass transition. Several material properties have this effect, such as plasticiser or moisture content [35], molecular weight [36] or the amount of catalyst used [37].

Fig. 9b,d shows that for a fixed location parameter ($\alpha = 6$), the slope of the curve changes with the change of the scale parameter (β), and the location of the inflexion point associated with the glass transition remains constant. β can be related to the rate of creep/relaxation process and can be used to take into account material properties that can affect the time course of the glass transition. This case is less common but can be used in specific areas such as polymer-substrate interaction studies [38].

3.5. Results of modelling for different types of polymers

By performing the modelling steps described in Section 3.3, the creep compliance and relaxation modulus models were obtained (Fig. 10a,b). The fitting parameters and the *NRMSE* value characterising the goodness of fit are given in Table 3. The fit was quite accurate in this normalised space, as the *NRMSE* value was less than 3 % in all cases examined. To quantify the accuracy of the resulting real-time model curve in describing the actual master curve, we introduced the δ_Y percent error (Eq. (10)):

$$\delta_Y = \frac{|Y_{TTS} - Y_{model}|}{Y_{TTS}} \cdot 100\ (\%), \tag{10}$$

where Y refers to the corresponding material characteristic $E(t)$ or $D(t)$, Y_{TTS} is the point on the $E(t)$ or $D(t)$ master curve at a given t time, and Y_{model} is the point on the corresponding model curve at the same t time. This was determined for each t value of the master curves, and a box plot of these values was constructed (Fig. 10c,d). The median value (δ_{median}) was used to characterise the overall accuracy of the model (Table 3).

The evolution of creep compliance has been projected for at least 32 years in all cases at $T_{ref} = 40$ °C. In the case of PLA creep, we only considered the data points of the TTS curve up to the glass transition region in modelling (up to 10^9 s).

Fig. 10c shows that the proposed modelling method can describe the evolution of creep compliance over a 32-year period for the tested PS, PLA and EPA materials, with a δ_{median} of 12.5, 8.0 and 1.5 %,

Table 4
Results of modelling for the plasticised composites with different composition.

		Modelling in the normalised field		Difference between TTS and model curve in real time
		Fitted parameters		δ_{median} (%)
		α	β	
Creep	PLA+CF30+OLA0	6.86	1.027	11.0
	PLA+CF30+OLA4	4.85	1.027 (fixed)	9.5
	PLA+CF30+OLA8	3.92	1.027 (fixed)	15.5
	PLA+CF30+OLA16	−0.98	1.027 (fixed)	9.3

respectively.

The evolution of the relaxation modulus for the thermoplastics at T_{ref} = 40 °C could only be predicted for 12 days with a δ_{median} of 16.4 % and 2.7 % for the PS and PLA, respectively. In the case of amorphous thermoplastic PS, the material softened to the point where it could no longer be tested. Therefore, at this T_{ref} temperature, the material was modelled to the limit of its application for this loading mode. In the case of semi-crystalline thermoplastic PLA, the shape of the curve changed significantly after the glass transition (10^6 s). On the log-log scale, the curve is no longer quasi-constant after the glass transition but has a rubbery plateau region with a high negative slope. In this case, the applied Gumbel model curve is no longer suitable for description.

This may be a problem for semi-crystalline thermoplastics because if the rubbery plateau region has a large slope, the model can only be applied until the glass transition region is reached. Thus, in the case of PLA, only the data up to 10^6 s were considered for modelling and error calculation. So, in the case of semi-crystalline thermoplastics, this method may only be suitable for decade-long predictions (on the logarithmic time scale) at temperatures much lower than T_g.

In the case of the thermosetting polymer (EPA), the δ_{median} for creep compliance and the relaxation modulus over the 32-year forecast was less than 2 %, which confirms that the model is an excellent tool for describing the creep and stress relaxation behaviour of thermosetting systems.

3.6. Results of modelling for plasticised composites with different composition

To explore the relationship between the model parameter and material properties, we also modelled the PLA + CF30 composites plasticised with 0, 4, 8 and 16 wt%. First, we performed the Gumbel distribution function-based modelling (described in Section 3.3) to the PLA + CF30 + OLA0 master curve. Then, the following parameters were fixed: D_{min}, D_{max}, β. These parameters can be fixed as experiments have shown that the plasticiser content does not affect the curve shapes, only shifts them along the x-axis. The location parameter for each plasticiser content was determined by iteration (in the D^*-t × field) until the δ_{median} value between the plasticised composite's $D(t)$ curve and the $D(t)$ model curve was minimised. Thus, we obtained different location parameters (α) (Table 4).

Fig. 11a and b show the model curves and the box plot of the percent errors of the modelling, respectively. After the glass transition region, the curves of the composites with 4 and 8 wt% OLA content have a monotonically increasing region with a high slope, which the Gumbel model is no longer suitable to describe. Therefore, in these two cases, we calculated the δ_Y error values only up to 10^5 s (corresponding to about 28 h). In the cases of the 0 wt% and 16 wt% cases, the δ_Y values were calculated for the total master curve. The δ_{median} was less than 16 % in every case.

Fig. 11c shows a strong linear relationship (R^2 = 0.98) between the

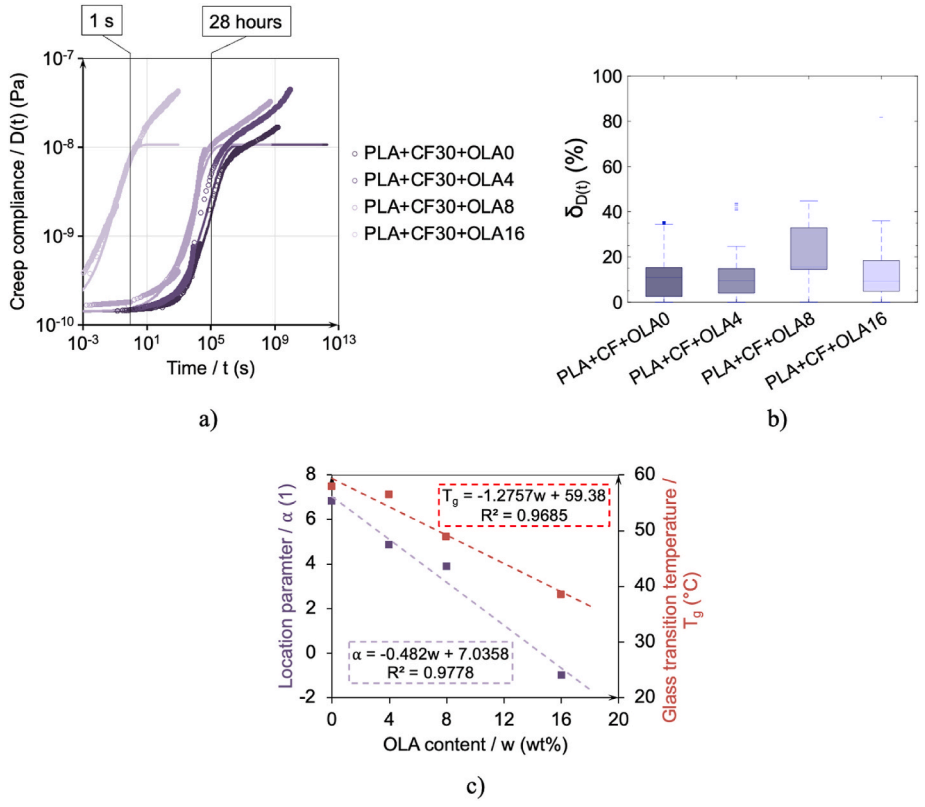

Fig. 11. Generated creep compliance master curves and models for plasticised composite materials in double logarithmic scale (a), box plots of percent error for creep models (b) and the quantitative relationship between scale parameter and plasticiser content (c). The empty circles denote the data points of the TTS curves, and the continuous lines represent the fitted models.

OLA content (w) and the location parameter (α). Consequently, using this quantitative relationship and the model curve of the reference (PLA + CF30 + OLA0), the creep compliance curve of the PLA + CF30 composites at $T = 40$ °C can be predicted for any OLA content between 0 wt % and 16 wt%. Furthermore, since the temperature dependence of the shift factors is also known (Fig. 7), and the OLA content did not affect this dependence significantly, the evolution of the creep compliance curve can be predicted at arbitrary temperatures between 22 °C and 70 °C.

Fig. 11c shows that the T_g also decreased trend-wise due to the plasticiser. Therefore, a similar relationship can be defined for any composition parameter that does not affect the shape of the creep/relaxation curve and only shifts the T_g trend-wise.

4. Conclusion

Creep and stress relaxation tests were performed on two thermoplastics (PS, PLA), a thermosetting polymer (EPA), and thermoplastic matrix composites with different plasticiser content (PLA + CF30 + OLA) at various temperatures. Then, using the test results, we constructed master curves at $T_{ref} = 40$ °C based on the temperature–time superposition (TTS) principle, and found that the Arrhenius model can properly describe the temperature dependence of the obtained shift factors in every case. We propose a suitable method to model the long-term evolution of the time-dependent creep compliance and relaxation modulus using a Gumbel CDF and CCDF model, respectively. The advantage of this method is that it is easy to use, as only two parameters need to be fitted; thus, complex optimisation algorithms are not required. For creep and stress relaxation master curves, the median percent error of modelling was less than 16 and 16.5 % in all cases, respectively. Furthermore, for the thermosetting EPA material, the median percent error for creep compliance and the relaxation modulus over the 32-year forecast was less than 2 %. Based on the low errors, we can conclude that this model can describe the creep and stress relaxation behaviour of thermosetting systems. In the case of the plasticised composites with different compositions, we found a strong linear relationship ($R^2 = 0.98$) between the OLA content and the location parameter of the Gumbel model. We also found that the plasticiser content did not affect the temperature dependence of the shift factors. We showed that based on the obtained relationships, the evolution of the creep compliance curve for any arbitrary OLA content (between 0 wt% and 16 wt%) at any desired temperature (between 22 °C and 70 °C) can be estimated. These results can facilitate the design of engineering structures incorporating components made of viscoelastic materials.

CRediT authorship contribution statement

Ábris Dávid Virág: Writing – original draft, Visualization, Validation, Methodology, Investigation, Formal analysis, Conceptualization. **Kolos Molnár:** Writing – review & editing, Supervision, Funding acquisition.

Declaration of competing interest

The authors declare that they have no known competing financial interests or personal relationships that could have appeared to influence the work reported in this paper.

Data availability

Data will be made available on request.

Acknowledgements

Project no. TKP-6-6/PALY-2021 has been implemented with the support provided by the Ministry of Culture and Innovation of Hungary from the National Research, Development and Innovation Fund, financed under the TKP2021-NVA funding scheme. Ábris Dávid Virág is thankful for the support of the EKÖP-24-4-I-BME-201 University Research Fellowship Programme of the Ministry for Culture and Innovation from the source of the National Research, Development and Innovation Fund. The research reported in this paper was supported by the National Research, Development and Innovation Office (FK 138501).

References

[1] K.F. Makris, J. Langeveld, F.H.L.R. Clemens, A review on the durability of PVC sewer pipes: research vs. practice, Struct. Infrastruct. Eng. 16 (2020) 880–897, https://doi.org/10.1080/15732479.2019.1673442.
[2] H.Y. Lee, J. Eoh, Securing integrity of high-temperature pressure boundary components in supercritical thermal plants with application of alternative design rules, Int. J. Pres. Ves. Pip. 195 (2022) 104598, https://doi.org/10.1016/J.IJPVP.2021.104598.
[3] P. Chellapandi, R. Srinivasan, S.C. Chetal, B. Raj, Experimental creep life assessment of tubular structures with geometrical imperfections in welds with reference to fast reactor plant life, Int. J. Pres. Ves. Pip. 83 (2006) 556–564, https://doi.org/10.1016/J.IJPVP.2006.03.009.
[4] A. Oseli, A. Aulova, M. Gergesova, I. Emri, Effect of temperature on mechanical properties of polymers, in: H. Altenbach, A. Öchsner (Eds.), Encyclopedia of Continuum Mechanics, Springer Berlin Heidelberg, Berlin, Heidelberg, 2019, pp. 1–20, https://doi.org/10.1007/978-3-662-53605-6_269-2.
[5] J.D. Ferry, Viscoelastic Properties of Polymers, third ed., John Wiley&Sons, New York, 1980.
[6] M.V. Ceron, D.L. Cecílio, R.V. Linn, S. Maghous, Nonlinear viscoelastic model for time-dependent mechanical characterization of PMMA acrylic bone cements, J. Mech. Behav. Biomed. Mater. 147 (2023) 106126, https://doi.org/10.1016/J.JMBBM.2023.106126.
[7] S.Z. Gebrehiwot, L. Espinosa-Leal, S.Z. Gebrehiwot, S.G. Fi, Characterising the linear viscoelastic behaviour of an injection moulding grade polypropylene polymer, Mech. Time-Dependent Mater. 26 (2021) 791–814, https://doi.org/10.1007/s11043-021-09513-0.
[8] L. Pálfi, K. Váradi, Characterization and implementation of the viscoelastic properties of an EPDM rubber into FEA for energy loss prediction, Period. Polytech. - Mech. Eng. 54 (2010) 35–40, https://doi.org/10.3311/pp.me.2010-1.06.
[9] E. Barrientos, F. Pelayo, Á. Noriega, M.J. Lamela, A. Fernández-Canteli, E. Tanaka, Optimal discrete-time Prony series fitting method for viscoelastic materials, Mech. Time-Dependent Mater. 23 (2019) 193–206, https://doi.org/10.1007/s11043-018-9394-z.
[10] Z. Cui, L.C. Brinson, A combination optimisation method for the estimation of material parameters for viscoelastic solids, Int. J. Comput. Sci. Math. 5 (2014) 325–335, https://doi.org/10.1504/IJCSM.2014.066443.
[11] A. Bonfanti, J.L. Kaplan, G. Charras, A. Kabla, Fractional viscoelastic models for power-law materials, Soft Matter 16 (2020) 6002–6020, https://doi.org/10.1039/d0sm00354a.
[12] M.R.M. Asyraf, M.R. Ishak, S.M. Sapuan, N. Yidris, R.A. Ilyas, Woods and composites cantilever beam: a comprehensive review of experimental and numerical creep methodologies, J. Mater. Res. Technol. 9 (2020) 6759–6776, https://doi.org/10.1016/j.jmrt.2020.01.013.
[13] J.J. Muñoz, S. Albo, Physiology-based model of cell viscoelasticity, Phys. Rev. E 88 (2013) 12708, https://doi.org/10.1103/PhysRevE.88.012708.
[14] B. Tajvidi Safa, C. Huang, A. Kabla, R. Yang, Active viscoelastic models for cell and tissue mechanics, R. Soc. Open Sci. 11 (2024) 231074, https://doi.org/10.1098/rsos.231074.
[15] J. Zhong, C. Yang, W. Ma, Z. Zhang, Long-term creep behavior prediction of polymethacrylimide foams using artificial neural networks, Polym. Test. 93 (2021), https://doi.org/10.1016/j.polymertesting.2020.106893.
[16] R.J. Young, P.A. Lovell (Eds.), Introduction to Polymers, third ed., CRC Press, New York, 2011.
[17] V. Binaz, K. Deepak, I. Singh, Comparative assessment of cutting processes in the mechanical behavior of basalt fiber/poly(lactic acid) matrix composites, Express Polym. Lett. 17 (2023) 152–168, https://doi.org/10.3144/expresspolymlett.2023.11.
[18] J. Gomez-Caturla, N. Montanes, L. Quiles-Carrillo, R. Balart, D. Garcia-Garcia, F. Dominici, D. Puglia, L. Torre, Development of biodegradable PLA composites and tangerine peel flour with improved toughness containing a natural-based terpenoid, Express Polym. Lett. 17 (2023) 789–805, https://doi.org/10.3144/expresspolymlett.2023.59.
[19] T. Tábi, K. Pölöskei, The effect of processing parameters and calcium-stearate on the ejection process of injection molded poly(lactic acid) products, Period. Polytech. - Mech. Eng. 66 (2022) 17–25, https://doi.org/10.3311/PPme.18246.
[20] T. Standau, C. Zhao, S.M. Castellón, C. Bonten, V. Altstädt, Chemical modification and foam processing of polylactide (PLA), Polymers 11 (2019), https://doi.org/10.3390/polym11020306.
[21] R. Petrény, C. Tóth, A. Horváth, L. Mészáros, Development of electrically conductive hybrid composites with a poly(lactic acid) matrix, with enhanced toughness for injection molding, and material extrusion-based additive manufacturing, Heliyon 8 (2022) e10287, https://doi.org/10.1016/j.heliyon.2022.e10287.

[22] H.M. Yoo, S.-Y. Jeong, S.-W. Choi, Analysis of the Rheological Property and Crystallization Behavior of Polylactic Acid (Ingeo™ Biopolymer 4032D) at Different Process Temperatures, vol. 21, 2021, pp. 702–709, https://doi.org/10.1515/epoly-2021-0071.
[23] Á.D. Virág, C. Tóth, L. Mészáros, Z. Juhász, Á. Bezerédi, R. Petrény, Optimizing the injection molding process for thermally and electrically conductive, carbon fiber and carbon nanotube-reinforced poly(lactic acid) hybrid composites with enhanced mechanical properties, J Appl Polym Sci n/a (2024) e56148, https://doi.org/10.1002/app.56148.
[24] D.W. Van Krevelen, K. Te Nijenhuis, Typology of polymers, in: D.W. Van Krevelen, K. Te Nijenhuis (Eds.), Properties of Polymers, fourth ed., Elsevier, Amsterdam, 2009.
[25] E. Zuza, J.M. Ugartemendia, A. Lopez, E. Meaurio, A. Lejardi, J.R. Sarasua, Glass transition behavior and dynamic fragility in polylactides containing mobile and rigid amorphous fractions, Polymer 49 (2008) 4427–4432, https://doi.org/10.1016/J.POLYMER.2008.08.012.
[26] L. Poh, E. Narimissa, M.H. Wagner, H.H. Winter, Interactive shear and extensional rheology—25 years of IRIS software, Rheol. Acta 61 (2022) 259–269, https://doi.org/10.1007/s00397-022-01331-6.
[27] A.P. Raman, M. Abou Anoma, L. Zhu, E. Rephaeli, S. Fan, Passive radiative cooling below ambient air temperature under direct sunlight. https://doi.org/10.1038/nature13883, 2014.
[28] T. Albers, A.H. Bonnett, Motor temperature considerations for pulp and paper mill applications, IEEE Trans. Ind. Appl. 38 (2002) 1701–1713, https://doi.org/10.1109/TIA.2002.805574.
[29] J. Lau, W. Bahnfleth, J. Freihaut, Estimating the effects of ambient conditions on the performance of UVGI air cleaners, Build. Environ. 44 (2009) 1362–1370, https://doi.org/10.1016/J.BUILDENV.2008.05.015.
[30] J. Dealy, D. Plazek, Time-temperature superposition-a users guide, Rheology Bulletin 78 (2009) 16–31. https://www.researchgate.net/publication/284663363.
[31] J.D. Peterson, S. Vyazovkin, C.A. Wight, Kinetics of the thermal and thermo-oxidative degradation of polystyrene, polyethylene and poly(propylene), Macromol. Chem. Phys. 202 (2001) 775–784, https://doi.org/10.1002/1521-3935(20010301)202:6<775::AID-MACP775>3.0.CO;2-G.
[32] Z. Alhulaybi, I. Dubdub, M. Al-Yaari, A. Almithn, A.F. Al-Naim, H. Aljanubi, Pyrolysis kinetic study of polylactic acid, Polymers 15 (2023), https://doi.org/10.3390/polym15010012.
[33] O. Konuray, J.M. Morancho, X. Fernández-Francos, M. García-Alvarez, X. Ramis, Curing kinetics of dually-processed acrylate-epoxy 3D printing resins, Thermochim. Acta 701 (2021) 178963, https://doi.org/10.1016/J.TCA.2021.178963.
[34] A. Álvarez-Vázquez, A. Fernández-Canteli, E. Castillo, F. Pelayo, M. Muñiz-Calvente, M.J. Lamela, A time- and temperature-dependent viscoelastic model based on the statistical compatibility condition, Mater. Des. 193 (2020), https://doi.org/10.1016/j.matdes.2020.108828.
[35] R. Petrény, L. Mészáros, Moisture dependent tensile and creep behaviour of multi-wall carbon nanotube and carbon fibre reinforced, injection moulded polyamide 6 matrix multi-scale composites, J. Mater. Res. Technol. 16 (2022) 689–699, https://doi.org/10.1016/J.JMRT.2021.12.030.
[36] H. Lee, L. Gu, D.J. Mooney, M.E. Levenston, O. Chaudhuri, Mechanical confinement regulates cartilage matrix formation by chondrocytes, Nat. Mater. 16 (2017) 1243–1251, https://doi.org/10.1038/nmat4993.
[37] J. Lou, S. Friedowitz, K. Will, J. Qin, Y. Xia, Predictably engineering the viscoelastic behavior of dynamic hydrogels via correlation with molecular parameters, Adv. Mater. 33 (2021) 2104460, https://doi.org/10.1002/adma.202104460.
[38] W. Zhang, J.F. Douglas, F.W. Starr, Effects of a “bound” substrate layer on the dynamics of supported polymer films, J. Chem. Phys. 147 (2017) 044901, https://doi.org/10.1063/1.4994064.